Robustness of terrestrial carbon and water cycle simulations against variations in spatial resolution

Christoph Müller[a,*†] and Wolfgang Lucht*

* Potsdam Institute for Climate Impact Research, PO Box 60 12 03, 14412 Potsdam, Germany

† International Max Planck Research School on Earth System Modeling, Bundesstr. 53, 20146 Hamburg, Germany

Running title: Robustness of DGVM simulations

[a] Corresponding author: e-mail address: Christoph.Mueller@pik-potsdam.de

Abstract

Dynamic Global Vegetation Models (DGVMs) of the terrestrial carbon and water cycle have been developed and validated at specific spatial resolutions (mostly 0.5°) but are increasingly being coupled to climate models at coarser spatial resolutions. Is this permissible? We ran the LPJ-DGVM at different spatial resolutions (0.5x0.5° to 10.0x10.0° in 0.5° intervals) to assess the robustness of terrestrial carbon and water flux simulations to changes in spatial resolution. We show that global model results are robust with only small deviations in the single-digit percent range from a benchmark run at 0.5°. The magnitude of the deviation increases with grid coarseness. Temporal dynamics are largely unaffected by grid cell size. The deviations from the benchmark are mostly spread evenly in space, and otherwise concentrated in areas with strong environmental gradients. We conclude that for coarse-resolution model coupling (such as with climate models) as well as for specific global-scale applications (such as global agroeconomic modeling or integrated assessment modeling) the spatial resolution of DGVMs can be reduced to coarser grids with little biogeochemical error.

1 Introduction

Models of terrestrial biogeochemistry and vegetation dynamics are increasingly being coupled to general circulation climate models (GCMs). The uncoupled versions for these terrestrial models, Dynamic Global Vegetation Models (DGVMs), however, have commonly been developed, operated and validated at a higher spatial resolution (typically 0.5°) than is usually the case for GCMs (several degrees typically). Are the simulated terrestrial carbon and water fluxes robust against this change of spatial resolution? The answer to this question is not just relevant to the use of DGVMs in GCMs but equally to the use of vegetation models in socioeconomically and agroeconomically oriented Integrated Assessment Models (IAMs), which equally lack high spatial resolution (typically they operate on 10-20 socioeconomic regions).

Process-based Dynamic Global Vegetation Models (DGVMs) are the state-of-the-art in simulating the global terrestrial biosphere. They are applied to studying the carbon cycle [Bachelet et al., 2001; Cramer et al., 2001; Dargaville et al., 2002; House et al., 2003; Woodward and Lomas, 2004; Schaphoff et al., 2006], the water cycle [Kucharik et al., 2000; Gerten et al., 2004; Leipprand and Gerten, 2006] and as land surface schemes in climate models [Foley et al., 1998; Cox et al., 2000; Joos et al., 2001; Dufresne et al., 2002; Brovkin et al., 2004; Krinner et al., 2005; Sitch et al., 2005; Friedlingstein et al., 2006]. DGVMs are applied at multiple spatial resolutions, ranging from 0.5x0.5° to 2.5x4.0° and beyond [Wang et al., 2004]. While the lower bound is determined by the resolution of suitable global climatological datasets, the upper bound is determined by the spatial resolution of coupled models, and/or computational requirements. If coupled to climate models, climate data may be downscaled to 0.5x0.5° resolution [e.g. Sitch et al., 2005] while DGVM output is aggregated to the climate models resolution [e.g. Foley et al., 1998]. Alternatively, the DGVM may be run at the spatial resolution of the climate model, avoiding up- and downscaling problems

[Foley et al., 1996; Brovkin et al., 1997; Cox, 2001]. This also speeds up the DGVM calculations, because the number of grid cells largely determines computation time. Thus, studies with high computational demands such as model intercomparisons [e.g. Cramer et al., 2001], sensitivity analyses [e.g. Zaehle et al., 2005] and scenario studies [e.g. Levy et al., 2004] are often performed at coarser spatial resolutions. DGVMs also need to be quickly computable in integrated assessment studies, because differences between participating modules in scale, data employed and simulation methods often require iterative procedures.

Although DGVMs are used at different resolutions, the robustness of their results against changes in spatial resolution has not been systematically investigated at the global scale. Suitability at different resolutions has mainly been assumed or derived from ad-hoc comparisons [e.g. Krinner et al., 2005]. Some DGVMs have been partially validated against global observations at specific coarser resolutions [e.g. Foley et al., 1996; Friend and White, 2000] and Wang et al. [2004] found very coarse resolutions (4.5x7.5°, R15) to be unsuitable. Much validation work is done against site data [Friend et al., 1997; Friend and White, 2000; Sitch et al., 2003; Zaehle et al., 2005] or at 0.5° resolution [Sitch et al., 2003; Le Toan et al., 2004]. The hydrology module of ORCHIDEE has been tested at different resolutions at a sub-continental scale [Verant et al., 2004]. The importance of vegetation heterogeneity at the km-scale for the dynamics of the Planetary Boundary Layer has been demonstrated by Woodward and Lomas [2001].

In this study, we investigate the effect of spatial resolution on global results of DGVMs, by simulating global vegetation dynamics with the LPJ model [Sitch et al., 2003; Gerten et al., 2004] at different regular grids, ranging from 0.5x0.5° to 10.0x10.0°. Since biogeochemical processes are represented in a comparable manner in other DGVMs [Cramer et al., 2001] it may be assumed that they will respond similarly to spatial aggregation of input data.

2 Methods

LPJ-DGVM

The LPJ Dynamic Global Vegetation Model (LPJ-DGVM) is a coupled biogeochemical-biogeographical process model that simulates global terrestrial vegetation and soil dynamics and the associated carbon and water fluxes [Sitch et al., 2003; Gerten et al., 2004]. For this, the processes of photosynthesis, evapotranspiration, and autotrophic and heterotrophic respiration, including the effects of soil moisture and drought stress, as well as a set of functional and allometric rules describing vegetation are implemented. Natural vegetation is represented by 10 different plant functional types (PFTs), of which 2 are herbaceous and 8 woody. Within each grid cell these may fractionally coexist. Their abundance is constrained by climatic conditions and by competition between the different PFTs for resources and space. Vegetation structure reacts dynamically to changes in climate, including invasion of new habitats and dieback. Fire disturbance is driven by a threshold litter load and soil moisture [Thonicke et al., 2001]. Photosynthesis, respiration, and the water balance are computed at a daily time step, while carbon allocation and vegetation dynamics are computed annually. For the daily time step, daily values of temperature, precipitation, and sunshine are computed internally from monthly climate input data. The model has been extensively tested against site [Sitch et al., 2003; Cramer et al., 2004; Gerten et al., 2005; Zaehle et al., 2005], inventory [Beer et al., 2006; Zaehle et al., 2006], satellite [Lucht et al., 2002; Wagner et al., 2003], atmospheric [Scholze et al., 2003; Sitch et al., 2003] and hydrological data [Gerten et al., 2004; Gerten et al., 2005].

Modeling protocol

We use LPJ results at the finest resolution available (0.5°x0.5°) as a benchmark to assess model results obtained at coarser spatial resolutions. For input, we use monthly data for mean

temperature, precipitation, number of wet days, and sunshine hours for 1901-2003, which are based on the CRU05 observations-derived climatology [New et al., 2000; Österle et al., 2003], atmospheric CO_2 concentrations [Keeling and Whorf, 2003], and soil classes derived from the FAO soil data set [Zobler, 1986; FAO, 1991].

To generate coarser resolution data, we aggregated the 0.5°-raster data for climate and soil in 0.5° intervals to regular grids ranging from 1.0°x1.0° to 10.0°x10.0° in spatial resolution (table 1), by averaging climate data weighted by area and using the dominant soil class. The total area simulated as land is equal for all grids by allowing for fractional areas. Atmospheric CO_2 concentrations are global values. The coarser grids can be positioned differently with respect to the finer baseline grid, which gives rise to a number of alternative aggregation schemes for each coarse resolution. We computed all possible alternatives for the resolutions 1.0° to 5.0° and one out of four alternatives for the regular grids of 5.5° to 10.0°, by shifting the grid 1° in latitudinal and/or longitudinal direction. Besides the regular resolutions of 1.0° to 10.0°, we also consider the 3.75°x2.5° resolution used by a number of climate models and by Joos et al. [2001], also in all alternative grid positions.

3 Results

The aggregation of data to coarser grids leads to a quadratic decrease in the number of grid cells and thus in computation time (table 1). It also leads to deviations from the benchmark run at 0.5° resolution. We compare the results of coarser resolution runs with the benchmark run regarding total global values (30-year averages, 1974-2003) of the transient run from 1901-2003, spatial patterns, and temporal variations of these global values.

Global values

The deviation from the benchmark values increases linearly with increasing coarseness. The slope of this increase is small (less than 1.5% per degree). Only the deviation of the net ecosystem exchange (NEE; here defined as soil respiration + fire emissions – net primary production (NPP)) does not increase strictly with coarseness but still displays a gentle linear trend. Figure 1 shows the deviation in percent of the benchmark value for selected model results. Annual runoff shows the largest deviations from the benchmark of all variables investigated (up to 14.2 percent at the coarsest resolution) and NEE the smallest (not more than 4.6 percent even for the coarsest resolution). The error bars in figure 1 show the standard deviation of the model results due to differences in grid positioning. It increases with cell size. For annual transpiration, interception, and runoff the grid position is of minor importance while it significantly affects the variation of deviations in NEE and fire emissions. Table 2 summarizes the slope of linear regression lines to the deviations from the benchmark and their coefficients of determination for each parameter; the intercept is zero in all cases. The small slopes (less than 1.5% per degree) indicate that simulation results are only slightly scaled with resolution. Large coefficients of determination (R^2) show that this scaling is strongly linear and that there are no qualitative shifts between different resolutions.

Spatial patterns

We compare values in each 0.5° grid cell of the benchmark run with their coarser-scale representatives in order to determine the effects of spatial resolution on the spatial pattern of deviations in each parameter. As shown exemplarily for annual transpiration in figure 2, the deviation from the benchmark is mostly distributed evenly in space (see also supplementary figures S1-S4 for maps of other variables). However, in areas with strong environmental gradients (i.e. borders of mountains, deserts etc.), coarser grid cells can differ substantially from the benchmark value. In these cases, substantially different temperature and/or precipitation values are averaged, canceling out extreme values. Thresholds for plant performance or existence may thus no longer be a factor in the aggregated climate data, with effects on the carbon and water cycles. With increasing coarseness of the grid, the number of these ill-represented cells increases and streaky latitudinal patterns emerge and become more prominent. These patterns derive from an overestimation of values at the coarser grid cell's sides towards the poles and an underestimation at the coarser grid cell's side that is pointing to the equator (or vice versa, depending on the parameter). Histograms of the deviation from the benchmark values show a bias towards enhanced plant performance, or a greener terrestrial biosphere (larger carbon uptake/pools, more evapotranspiration and interception, less runoff) that emerges and increases with coarseness of the grid (see figure 3 for an exemplary histogram of annual runoff and supplementary figures S5-S7). Table 3 represents the correlation coefficient of the spatial pattern at the benchmark resolution with those at coarser resolutions. Values of 1 indicate perfect correlation (here: similarity) of the spatial patterns, while values of 0 represent no correlation at all.

Temporal dynamics

The temporal dynamics of model results are hardly affected by the grid's resolution. The interannual variation is almost identical for all grids but their intercepts differ (values increase

linearly with grid coarseness, see above). Correlation coefficients of the correlations between the time series of the benchmark run and corresponding time series at coarser resolutions range between 1.0 and 0.84 (1.0 to 0.93 for resolutions up to 5.0°), expressing their strong similarity. Figure 4 exemplarily shows the time series of NPP at different resolutions (see supplementary figures S8-S10 for time series of the other output variables).

4 Discussion

We find that overall, model results are surprisingly robust against changes in spatial resolutions from 0.5° to 10°. They show a persistent linear trend with larger deviations at larger resolutions, but the slope is small. There are no climate input data available at finer spatial resolutions than 0.5°, inhibiting an exploration of this trend at finer resolutions. The 0.5° grid is often used in DGVM studies – but for historical and not scientific reasons. This is also demonstrated here: The 0.5° resolution does not differ qualitatively from coarser resolutions. Utilizing the 0.5° grid as a benchmark may thus be debatable but can be justified by the extensive validation of LPJ, the DGVM used here, at this spatial resolution.

There are two major possible explanations for the weak influence of spatial resolution on DGVM results: First, the 0.5° resolution may already be too coarse to account for relevant effects of spatial heterogeneity. The climate data set used, as the main driver of the model, is interpolated from point measurements to the 0.5° grid. Thus, spatial climate patterns may be artificially smoothed and can therefore be aggregated to coarser resolutions without substantial information loss. Second, LPJ here considers, as most DGVM do at the global scale, the state of natural vegetation. Woodward and Lomas [2001] demonstrated that differences in land-cover type at the km-scale affect the biogeophysical interaction between vegetation and the atmosphere. Assuming potential natural vegetation, forests are the dominant land-cover types, while grasslands, savannas, and deserts only exist under specific climate conditions. Along the borders between these land-cover types (e.g. Sahara desert, mountain ranges), we also observe larger effects of spatial resolution on the carbon and water cycles (see figure 2 and supplementary figures S1-S4).

Despite the weak impact of spatial resolution at the global level, differences between the benchmark run at 0.5° resolution and simulations at coarser grids occur. The deviation of the global values only partially reflect the deviations at grid cell level, since these include both

negative and positive deviations and are largely compensated in the global values. Streaky patterns for example emerge and grow at coarser spatial resolutions. They reflect the importance of solar radiation, which is computed as a function of latitude for cell centers in our model. Within a coarse cell, the insolation of the cell's center is used for the entire grid cell, leading to over- and underestimated insolation values at its borders. However, such finer-scale deviations are compensated overall within each coarser grid cell.

On the other hand, averaging within a coarse grid cell of extreme climatic conditions that are unfavorable for vegetation growth, such as aridity, with less extreme conditions in neighboring areas increases total vegetation growth at the coarse scale. Averaging the opposite extreme, in this case high humidity, with less extreme neighboring cells, does not normally compensate for this effect within each coarse grid cell. As a consequence, the terrestrial biosphere becomes "greener" or more productive at coarser spatial resolutions. Model results at coarser spatial resolutions can therefore not necessarily be interpreted locally or regionally but need to be carefully analyzed with respect to the softening of extremes in the process of spatial aggregation.

The temporal dynamics of model results are barely affected by grid coarseness. Hence, model results may need some scaling to match, for example, observed values, but their reaction to climatic fluctuations – and thus their interannual variation – remain largely unaffected. Coupling DGVMs to climate or other models is therefore not problematic in this respect.

We here studied biogeochemical cycles only and cannot judge the effects of grid coarseness on biophysical parameters such as on albedo and energy fluxes. These may well be affected by grid coarseness in coupled DGVM-climate model applications, causing additional feedbacks on biogeochemical cycles. Systematic testing of these effects would require a coupled climate-vegetation model that can be run at fine spatial resolution (see Woodward and Lomas [2001], for an example at the km-scale).

Based on these results, the choice of a spatial resolution suitable for a specific DGVM application is not straightforward. There is no threshold resolution above which model results begin to markedly deviate from the benchmark values. Overall, the uncertainty present in recently published estimates for carbon fluxes [Schimel et al., 2001; Bopp et al., 2002; Plattner et al., 2002] and pools [Post et al., 1982; Olson et al., 1985; Eswaran et al., 1993; Batjes, 1996; WBGU, 1998; Saugier et al., 2001] is with error ranges of up to 50 percent significantly larger than the deviations found here due to grid coarseness, rendering coarse-resolution terrestrial carbon cycle simulations suitable to investigations of processes. In contrast, published hydrological estimates vary by roughly +/- 10% [Gerten et al., 2004], a level of uncertainty smaller than the deviation found, for runoff, for grids coarser than 7.0x7.0°.

Regular grids are an arbitrary choice of gridding pattern. The world is characterized by spatial heterogeneity. Regular grids average smaller-scale differences and artificially separate larger homogenous (in terms of the characteristics of interest) areas. Consequently, polygonal or irregular grids that are based, for example, on the spatial patterns of factors that determine plant growth should – in principle – be able to reproduce the model's benchmark run with a smaller number of grid cells. We performed several such experiments and find that the error incurred for irregular grids, in comparison to the benchmark, is dominated by the error incurred for the largest cell of the irregular grid. The overall deviation is found to be larger than that of a regular grid with the same number of grid cells. The reason is that deviations generally increase exponentially with pixel size, with an exponent that is larger than unity. Hence for grids with varying cell size, the error of large cells enters the global error with large values than that of small cells. The largest cells dominate the deviation of irregular grids from the benchmark. Regular grids therefore always produce smaller deviations than irregular grids with the same number of grid cells. We conclude that irregular patterns, even when selected to

follow natural patterns such as climate or vegetation zones, are not an advantage over regular grids in terms of their ability to provide accuracy in coarse-scale simulations.

Our study does not investigate whether the benchmark simulation is accurate in comparison to data. Rather, we investigated whether results depend on spatial resolution. The model we used was the LPJ DGVM but processes in most DGVMs are implemented in a broadly similar manner [Foley et al., 1996; Brovkin et al., 1997; Friend and White, 2000; Cox, 2001; Sitch et al., 2003; Woodward and Lomas, 2004; Krinner et al., 2005]; see also Cramer et al. [2001] and Le Toan et al. [2004]. It is therefore reasonable to assume that our findings will hold for other DGVMs as well.

5 Conclusions

The spatial resolution of DGVM simulations can be much reduced for specific global applications since model results are largely robust to changes in spatial resolution, with deviations from a full-resolution run of less than 5 percent in most variables even for very coarse resolutions. However, specific cells and areas with strong environmental gradients cannot be represented well at coarser resolutions. Coupling of DGVMs to models that operate a coarser grids, such as climate models, is unproblematic with respect to the temporal dynamics of DGVMs, which are mainly unaffected by spatial resolution. Especially applications with a focus on regional/local criteria need to balance the error in the representation of single cells and gradients with the benefits of coarser grids such as reduced computational demands. Irregular spatial grids should be explored for the best trade off between computation time and spatial accuracy.

Acknowledgements

CM was supported by the International Max Planck Research School on Earth System Modelling, Hamburg, Germany, WL by the Leibniz Association's Pakt für Forschung project "Biosphere and Society Under Global Change". We thank Victor Brovkin, Dieter Gerten, and Wolfgang Cramer for valuable discussions and support.

References

Bachelet, D., R. P. Neilson, J. M. Lenihan and R. J. Drapek (2001), Climate change effects on vegetation distribution and carbon budget in the United States, *Ecosystems 4*(3), 164-185.

Batjes, N. H. (1996), Total carbon and nitrogen in the soils of the world, *European Journal of Soil Science 47*(2), 151-163.

Beer, C., W. Lucht, C. Schmullius and A. Shvidenko (2006), Small net carbon dioxide uptake by Russian forests during 1981-1999, *Geophys. Res. Lett. 33*, L15403, doi:10.1029/2006GL026919.

Bopp, L., C. Le Quere, M. Heimann, A. C. Manning and P. Monfray (2002), Climate-induced oceanic oxygen fluxes: Implications for the contemporary carbon budget, *Global Biogeochem. Cycles 16*(2).

Brovkin, V., A. Ganopolski and Y. Svirezhev (1997), A continuous climate-vegetation classification for use in climate-biosphere studies, *Ecological Modelling 101*(2-3), 251-261.

Brovkin, V., S. Sitch, W. von Bloh, M. Claussen, E. Bauer and W. Cramer (2004), Role of land cover changes for atmospheric CO_2 increase and climate change during the last 150 years, *Global Change Biol. 10*(8), 1253-1266.

Cox, P. M. (2001), Description of the "TRIFFID" Dynamic Global Vegetation Model, Technical Note 24, Hadley Centre, Met Office, pp. 17 Berks, UK.

Cox, P. M., R. A. Betts, C. D. Jones, S. A. Spall and I. J. Totterdell (2000), Acceleration of global warming due to carbon-cycle feedbacks in a coupled climate model, *Nature 408*(6813), 184-187.

Cramer, W., A. Bondeau, S. Schaphoff, W. Lucht, B. Smith and S. Sitch (2004), Tropical forests and the global carbon cycle: impacts of atmospheric carbon dioxide, climate

change and rate of deforestation, *Philos. Trans. R. Soc. London Ser. B 359*(1443), 331-343.

Cramer, W., A. Bondeau, F. Woodward, I. Prentice, R. Betts, V. Brovkin, P. Cox, V. Fisher, J. Foley, A. Friend, C. Kucharik, M. Lomas, N. Ramankutty, S. Sitch, B. Smith, A. White and C. Young-Molling (2001), Global response of terrestrial ecosystem structure and function to CO_2 and climate change: results from six dynamic global vegetation models, *Global Change Biol. 7*(4), 357-373.

Dargaville, R. J., M. Heimann, A. D. McGuire, I. C. Prentice, D. Kicklighter, F. Joos, J. S. Clein, G. Esser, J. Foley, J. Kaplan, R. A. Meier, J. M. Melillo, B. Moore III, N. Ramankutty, T. Reichenau, A. Schloss, S. Sitch, H. Tian, L. J. Williams and U. Wittenberg (2002), Evaluation of terrestrial carbon cycle models with atmospheric CO_2 measurements: Results from transient simulations considering increasing CO_2, climate, and land-use effects, *Global Biogeochem. Cycles 16*(4), 1092, doi:10.1029/2001GB001426.

Dufresne, J.-L., P. Friedlingstein, M. Berthelot, L. Bopp, P. Ciais, L. Fairhead, H. Le Treut and P. Monfray (2002), On the magnitude of positive feddback between future climate change and the carbon cycle, *Geophys. Res. Lett. 29*(10), 1405, doi:10.1029/2001GL013777.

Eswaran, H., E. van den Berg and P. Reich (1993), Organic carbon in soils of the World, *Soil Sci. Soc. Am. J. 57*(1), 192-194.

FAO (1991), The Digitized Soil Map of the World (Release 1.0), World Soil Resources Report 67/1, Food and Agriculture Organization of the United Nations.

Foley, J. A., S. Levis, I. C. Prentice, D. Pollard and S. L. Thompson (1998), Coupling dynamic models of climate and vegetation, *Global Change Biol. 4*(5), 561-579.

Foley, J. A., I. C. Prentice, N. Ramankutty, S. Levis, D. Pollard, S. Sitch and A. Haxeltine (1996), An integrated biosphere model of land surface processes, terrestrial carbon balance, and vegetation dynamics, *Global Biogeochem. Cycles 10*(4), 603-628.

Friedlingstein, P., P. Cox, R. A. Betts, L. Bopp, W. von Bloh, V. Brovkin, P. Cadule, S. Doney, M. Eby, I. Fung, G. Bala, J. John, C. D. Jones, F. Joos, T. Kato, M. Kawamiya, W. Knorr, K. Lindsay, H. D. Matthews, T. Raddatz, P. Rayner, C. Reick, E. Roeckner, K.-G. Schnitzler, R. Schnur, K. Strassmann, A. J. Weaver, C. Yoshikawa and N. Zeng (2006), Climate-carbon cycle feedback analysis, results from the C^4MIP model intercomparison, *Journal of Climate 19*(14), 3337-3353.

Friend, A. D. and A. White (2000), Evaluation and analysis of a dynamic terrestrial ecosystem model under preindustrial conditions at the global scale, *Global Biogeochem. Cycles 14*(4), 1173-1190.

Friend, A. D., A. K. Stevens, R. G. Knox and M. G. R. Cannell (1997), A process-based, terrestrial biosphere model of ecosystem dynamics (Hybrid v3.0), *Ecological Modelling 95*(2-3), 249-287.

Gerten, D., S. Schaphoff, U. Haberlandt, W. Lucht and S. Sitch (2004), Terrestrial vegetation and water balance - hydrological evaluation of a dynamic global vegetation model, *Journal of Hydrology 286*(1-4), 249-270.

Gerten, D., W. Lucht, S. Schaphoff, W. Cramer, T. Hickler and W. Wagner (2005), Hydrologic resilience of the terrestrial biosphere, *Geophys. Res. Lett. 32*(21).

House, J. I., I. C. Prentice, N. Ramankutty, R. A. Houghton and M. Heimann (2003), Reconciling apparent inconsistencies in estimates of terrestrial CO_2 sources and sinks, *Tellus Series B-Chemical and Physical Meteorology 55*(2), 345-363.

Joos, F., I. C. Prentice, S. Sitch, R. Meyer, G. Hooss, G. K. Plattner, S. Gerber and K. Hasselmann (2001), Global warming feedbacks on terrestrial carbon uptake under the

Intergovernmental Panel on Climate Change (IPCC) emission scenarios, *Global Biogeochem. Cycles 15*(4), 891-907.

Keeling, C. D. and T. P. Whorf (2003), Atmospheric CO_2 records from sites in the SIO air sampling network. In Trends: A Compendium of Data on Global Change. Carbon Dioxide Information Analysis Center, Oak Ridge National Laboratory, U.S. Department of Energy Oak Ridge, Tenn., U.S.A.

Krinner, G., N. Viovy, N. de Noblet-Ducoudre, J. Ogee, J. Polcher, P. Friedlingstein, P. Ciais, S. Sitch and I. C. Prentice (2005), A dynamic global vegetation model for studies of the coupled atmosphere-biosphere system, *Global Biogeochem. Cycles 19*(1).

Kucharik, C. J., J. A. Foley, C. Delire, V. A. Fisher, M. T. Coe, J. D. Lenters, C. Young-Molling, N. Ramankutty, J. M. Norman and S. T. Gower (2000), Testing the performance of a Dynamic Global Ecosystem Model: Water balance, carbon balance, and vegetation structure, *Global Biogeochem. Cycles 14*(3), 795-825.

Le Toan, T., S. Quegan, I. Woodward, M. Lomas, N. Delbart and G. Picard (2004), Relating Radar Remote Sensing of Biomass to Modelling of Forest Carbon Budgets, *Climatic Change 67*(2), 379-402.

Leipprand, A. and D. Gerten (2006), Global effects of doubled atmospheric CO_2 content on evapotranspiration, soil moisture and runoff under potential natural vegetation, *Hydrological Sciences Journal-Journal Des Sciences Hydrologiques 51*(1), 171-185.

Levy, P. E., A. D. Friend, A. White and M. G. R. Cannell (2004), The Influence of Land Use Change On Global-Scale Fluxes of Carbon from Terrestrial Ecosystems, *Climatic Change 67*(2), 185-209.

Lucht, W., I. C. Prentice, R. B. Myneni, S. Sitch, P. Friedlingstein, W. Cramer, P. Bousquet, W. Buermann and B. Smith (2002), Climatic Control of the High-Latitude Vegetation Greening Trend and Pinatubo Effect, *Science 296*(5573), 1687-1689.

New, M. G., M. Hulme and P. D. Jones (2000), Representing twentieth-century space-time climate variability. Part II: Development of 1901-1996 monthly grids of terrestrial surface climate, *Journal of Climate 13*, 2217-2238.

Olson, J., J. A. Watts and L. J. Allison (1985), Major world ecosystem complexes ranked by carbon in live vegetation: A database, Carbon Dioxide Information Center, Oak Ridge National Laboratory Oak Ridge, Tennessee.

Österle, H., F.-W. Gerstengarbe and P. C. Werner (2003), Homogenisierung und Aktualisierung des Klimadatensatzes der Climate Research Unit der Universität of East Anglia, Norwich, *Terra Nostra 6*.

Plattner, G. K., F. Joos and T. F. Stocker (2002), Revision of the global carbon budget due to changing air-sea oxygen fluxes, *Global Biogeochem. Cycles 16*(4).

Post, W. M., W. R. Emanuel and P. J. Zinke (1982), Soil carbon pools and world life zones, *Nature 298*(5870), 156-159.

Saugier, B., J. Roy and H. A. Mooney (2001), Estimations of global terrestrial productivity: converging toward a single number?, in *Terrestrial Global Productivity* edited by Roy, J., B. Saugier and H. A. Mooney, Academic Press, San Diego.

Schaphoff, S., W. Lucht, D. Gerten, S. Sitch, W. Cramer and I. C. Prentice (2006), Terrestrial biosphere carbon storage under alternative climate projections, *Climatic Change*, doi:10.1007/s10584-005-9002-5.

Schimel, D., J. House, K. Hibbard, P. Bousquet, P. Ciais, P. Peylin, B. Braswell, M. Apps, D. Baker, A. Bondeau, J. Canadell, G. Churkina, W. Cramer, A. Denning, C. Field, P. Friedlingstein, C. Goodale, M. Heimann, R. Houghton, J. Melillo, B. Moore, D. Murdiyarso, I. Noble, S. Pacala, I. Prentice, M. Raupach, P. Rayner, R. Scholes, W. Steffen and C. Wirth (2001), Recent patterns and mechanisms of carbon exchange by terrestrial ecosystems, *Nature 414*(6860), 169-172.

Scholze, M., J. Kaplan, W. Knorr and M. Heimann (2003), Climate and interannual variability of the atmosphere-biosphere $^{13}CO_2$ flux, *Geophys. Res. Lett. 30*(2), doi:10.1029/2002GL015631.

Sitch, S., V. Brovkin, W. von Bloh, D. van Vuuren, B. Eickhout and A. Ganopolski (2005), Impacts of future land cover changes on atmospheric CO_2 and climate., *Global Biogeochem. Cycles 19*(GB2013), doi:10.1029/2004GB002311.

Sitch, S., B. Smith, I. Prentice, A. Arneth, A. Bondeau, W. Cramer, J. Kaplan, S. Levis, W. Lucht, M. Sykes, K. Thonicke and S. Venevsky (2003), Evaluation of ecosystem dynamics, plant geography and terrestrial carbon cycling in the LPJ dynamic global vegetation model, *Global Change Biol. 9*(2), 161-185.

Thonicke, K., S. Venevsky, S. Sitch and W. Cramer (2001), The role of fire disturbance for global vegetation dynamics: coupling fire into a Dynamic Global Vegetation Model, *Global Ecology & Biogeography 10*, 661-677.

Verant, S., K. Laval, J. Polcher and M. De Castro (2004), Sensitivity of the continental hydrological cycle to the spatial resolution over the Iberian Peninsula, *Journal of Hydrometeorology 5*(2), 267-285.

Wagner, W., K. Scipal, C. Pathe, D. Gerten, W. Lucht and B. Rudolf (2003), Evaluation of the agreement between the first global remotely sensed soil moisture data with model and precipitation data, *Journal of Geophysical Research-Atmospheres 108*(D19).

Wang, G., E. A. B. Eltahir, J. A. Foley, D. Pollard and S. Levis (2004), Decadal variability of rainfall in the Sahel: results from the coupled GENESIS-IBIS atmosphere-biosphere model, *Climate Dynamics 22*(6 - 7), 625-637.

WBGU (1998), The accounting of biological sinks and sources under the Kyoto Protocol - A step forwards or backwards for global environmental protection?, WBGU Special Report, pp. 75 Bremerhaven, Germany.

Woodward, F. I. and M. R. Lomas (2001), Integrating fluxes from heterogeneous vegetation, *Global Ecology and Biogeography 10*(6), 595-601.

Woodward, F. I. and M. R. Lomas (2004), Vegetation dynamics - simulating responses to climatic change, *Biological Reviews 79*(3), 643-670.

Zaehle, S., S. Sitch, B. Smith and F. Hatterman (2005), Effects of parameter uncertainties on the modeling of terrestrial biosphere dynamics, *Global Biogeochem. Cycles 19*(GB3020), doi:10.1029/2004GB002395.

Zaehle, S., S. Sitch, I. C. Prentice, J. Liski, W. Cramer, M. Erhard, T. Hickler and B. Smith (2006), The importance of age-related decline of forest NPP for modeling regional carbon balances, *Ecological Applications 16*(4).

Zobler, L. (1986), A World Soil File for Global Climate Modelling, NASA technical memorandum 87802, NASA, pp. 32 Washington, D.C.

Figures

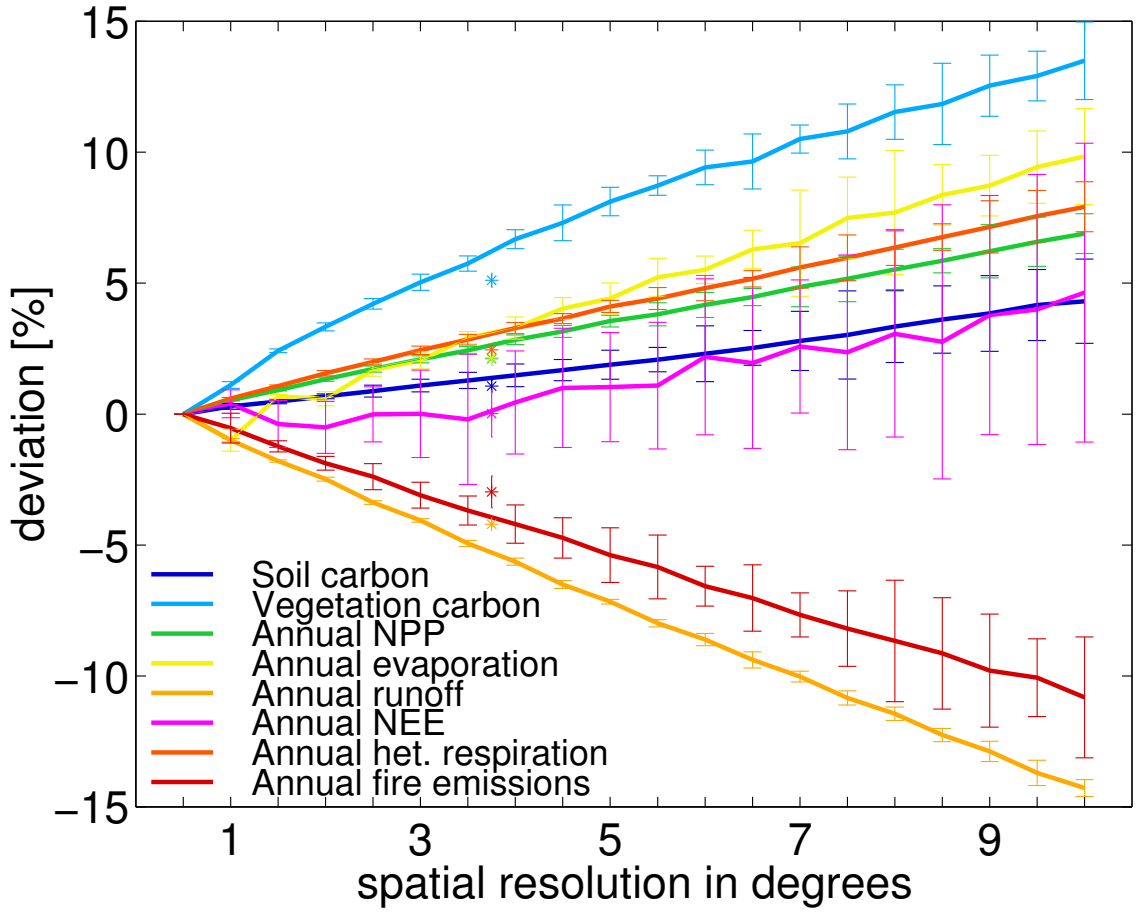

Figure 1. Percent deviation from benchmark run of selected results at different regular grids. The deviation of the regular 2.5x3.75° grid is shown as asterisks. The error bars show the standard deviation of the model results due to differences in grid positioning.

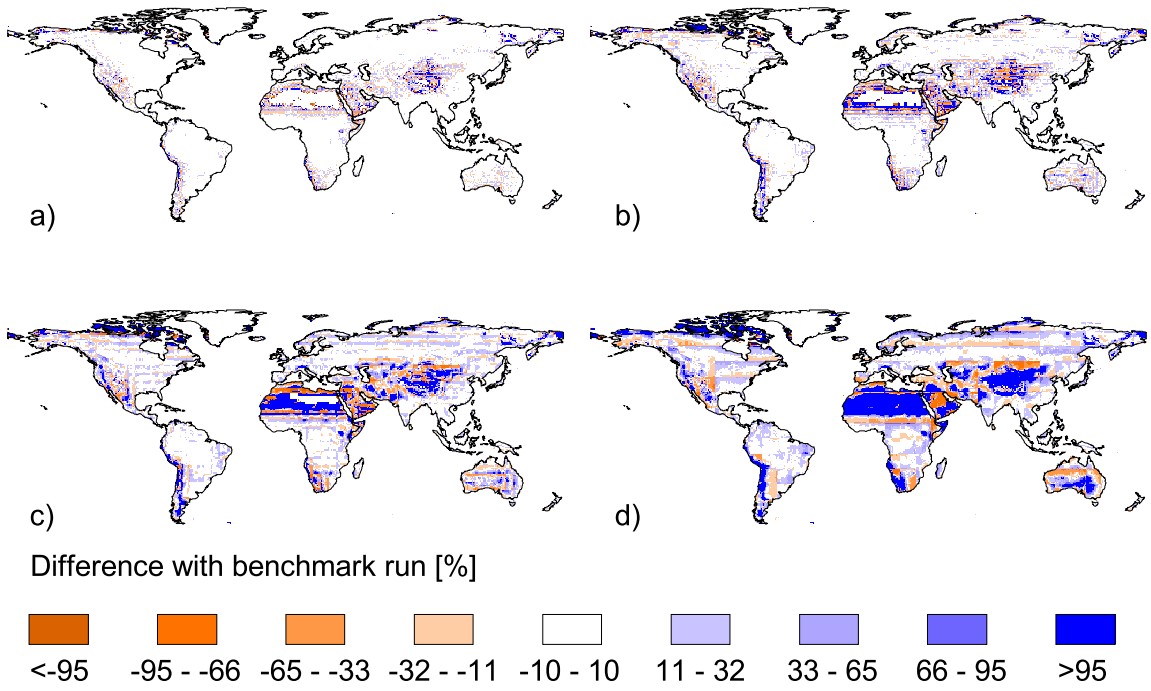

Figure 2. Map of pixel deviation of annual transpiration from benchmark at (a) 1.0, (b) 2.5, (c) 5.0, and (d) 10.0. Note that large increases (dark blue) in areas with very low transpiration (e.g., deserts) in the benchmark run may be low increases in absolute numbers.

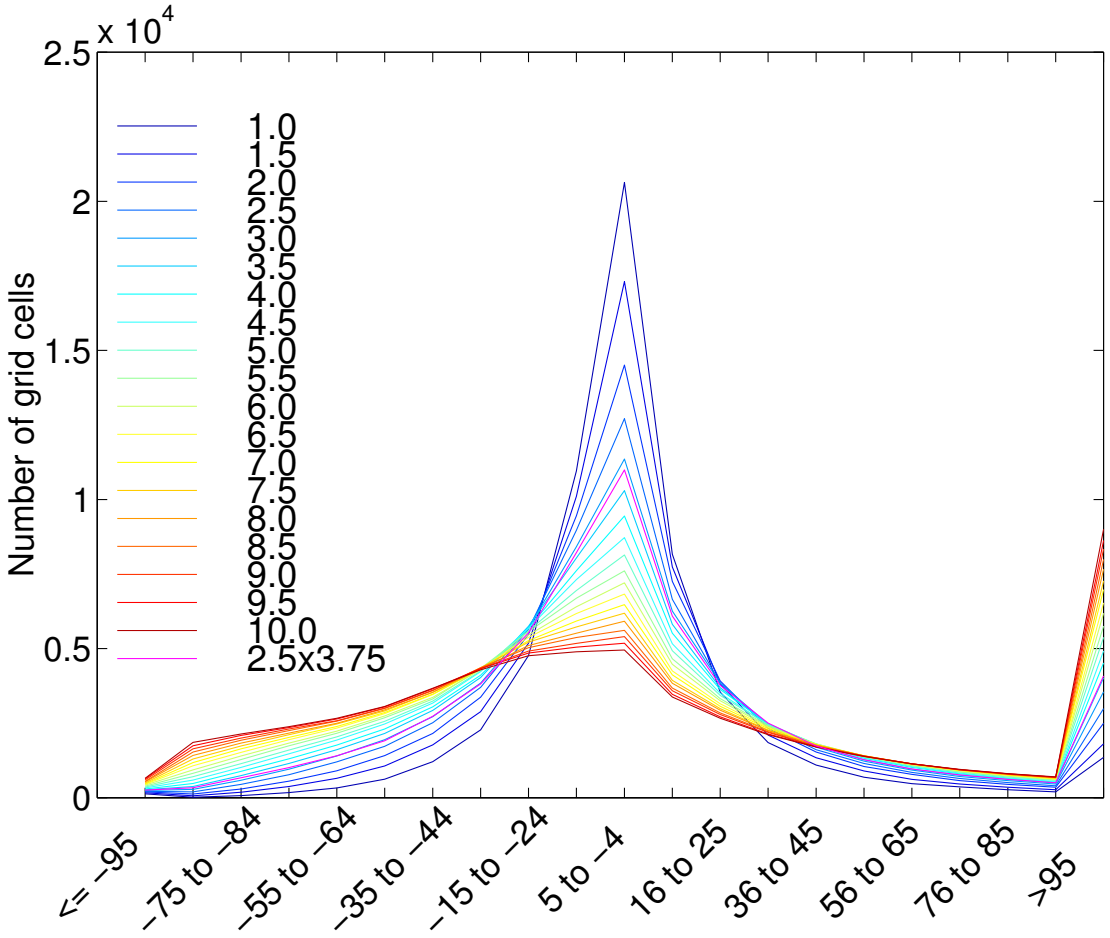

Figure 3. Histogram of difference between each 0.5° grid cell and their corresponding coarser grid cell in percent, exemplary for annual runoff.

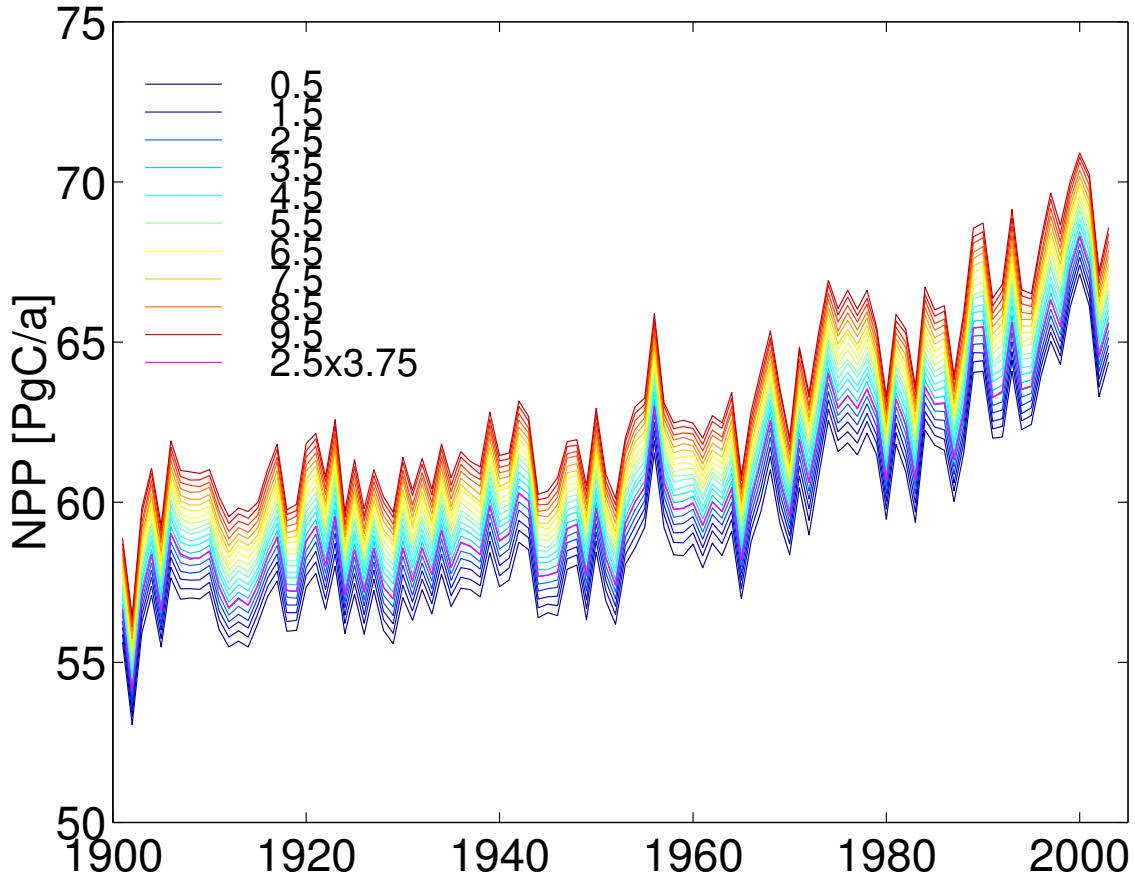

Figure 4. Time series of NPP at different resolutions. Note that all resolutions are shown in the figure, while the legend is reduced to every second grid; NPP increases linearly with grid coarseness.

Supplementary figure S1. Map of pixel deviation of annual runoff (I), interception (II), and evaporation (III) from benchmark at (a) 1.0, (b) 2.5, (c) 5.0, and (d) 10.0.
Note that large increases (dark blue) in areas with very low values (e.g. deserts) in the benchmark run may be low increases in absolute numbers.

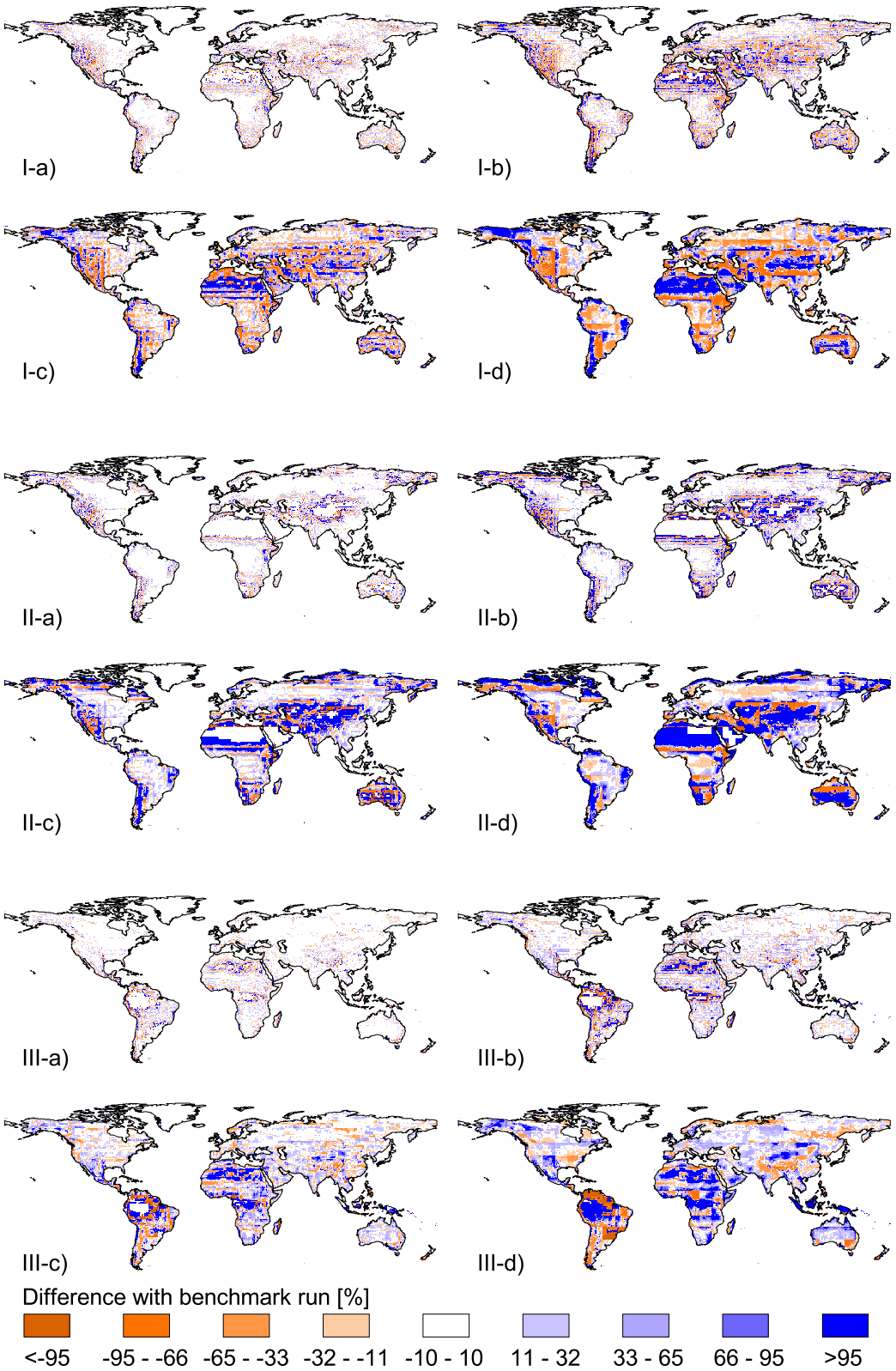

Supplementary figure S2. Map of pixel deviation of vegetation (I), litter (II), and soil carbon (III) from benchmark at (a) 1.0, (b) 2.5, (c) 5.0, and (d) 10.0.
Note that large increases (dark green) in areas with very low values (e.g. deserts) in the benchmark run may be low increases in absolute numbers.

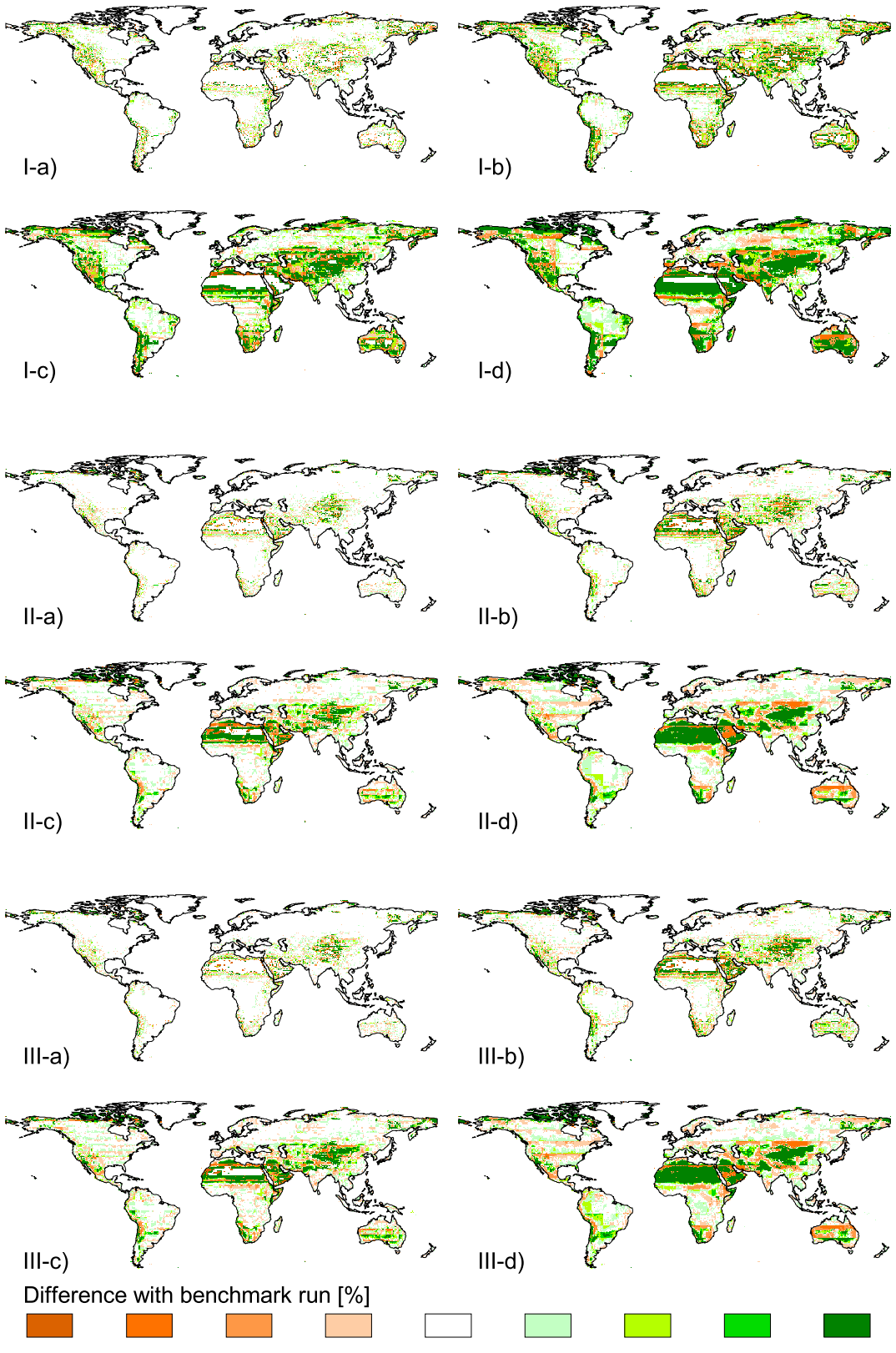

Supplementary figure S3. Map of pixel deviation of soil respiration (I) and NPP (II) from benchmark at (a) 1.0, (b) 2.5, (c) 5.0, and (d) 10.0.
Note that large increases (dark green) in areas with very low values (e.g. deserts) in the benchmark run may be low increases in absolute numbers.

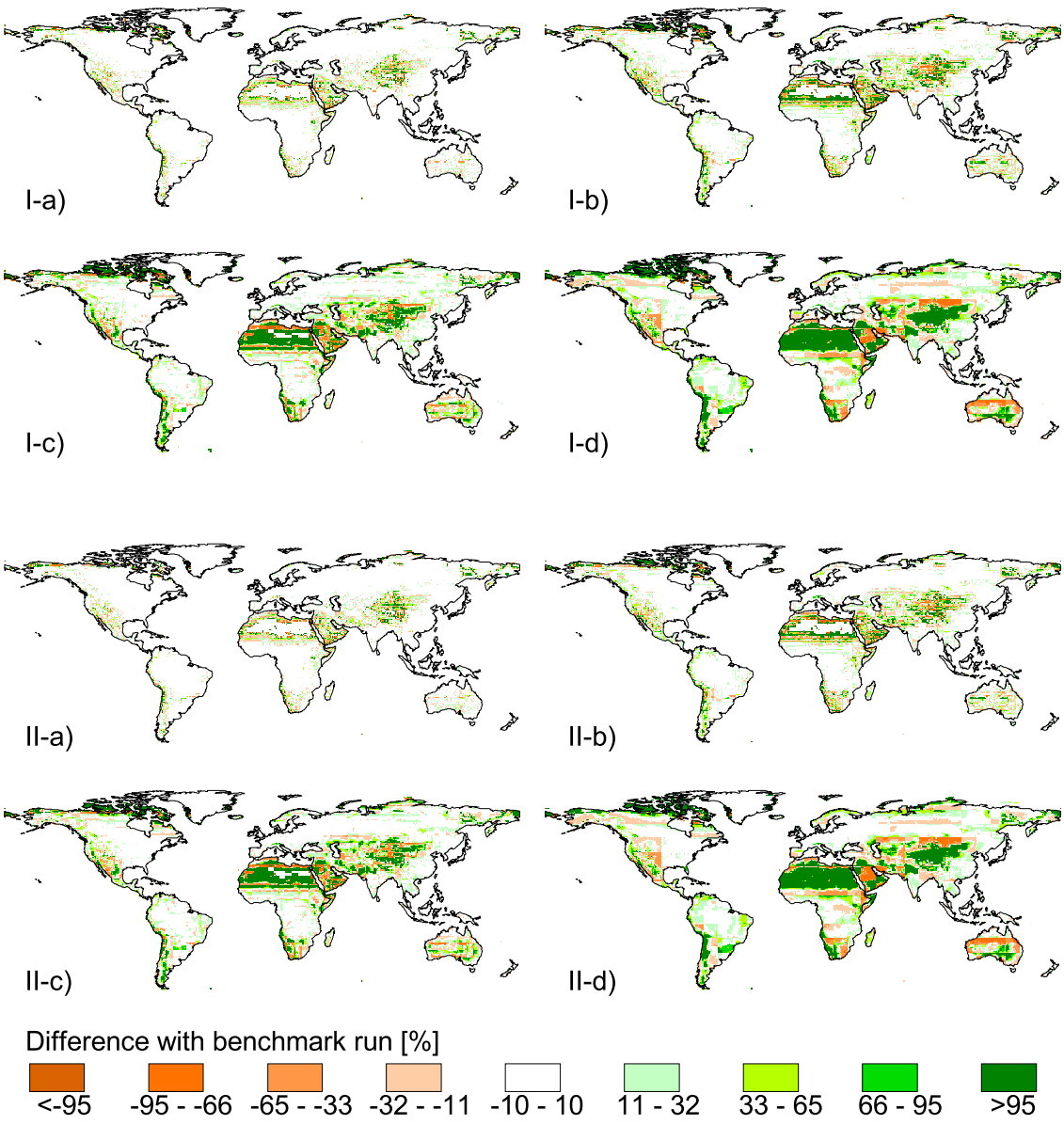

Supplementary figure S4. Map of pixel deviation of fire emissions (I) and
NEE (II) from benchmark at (a) 1.0, (b) 2.5, (c) 5.0, and (d) 10.0.
Note that large increases (dark green) or decreases (dark orange) in areas with very small values (e.g. deserts) in the benchmark run may be low increases/decreases in absolute numbers.

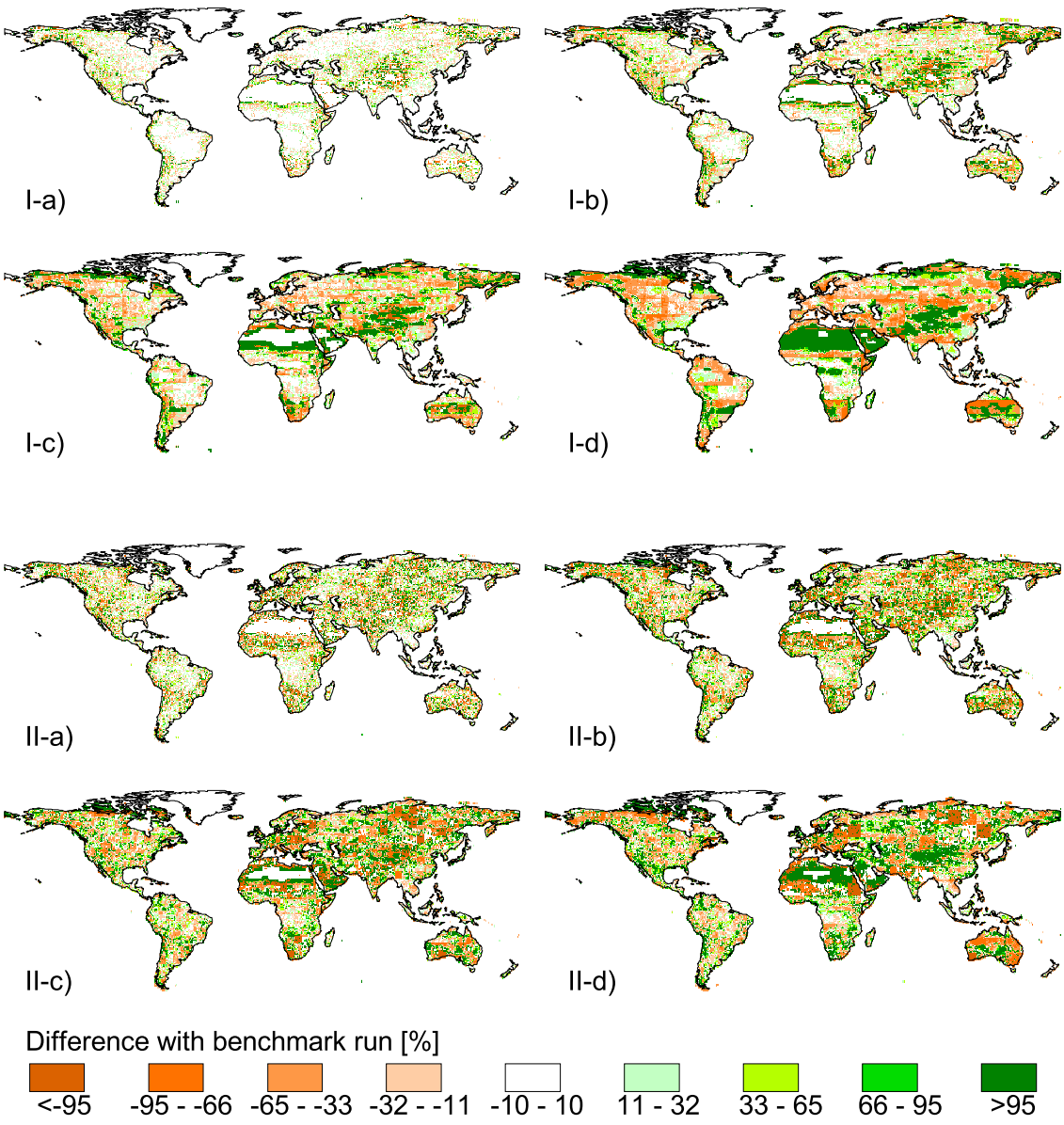

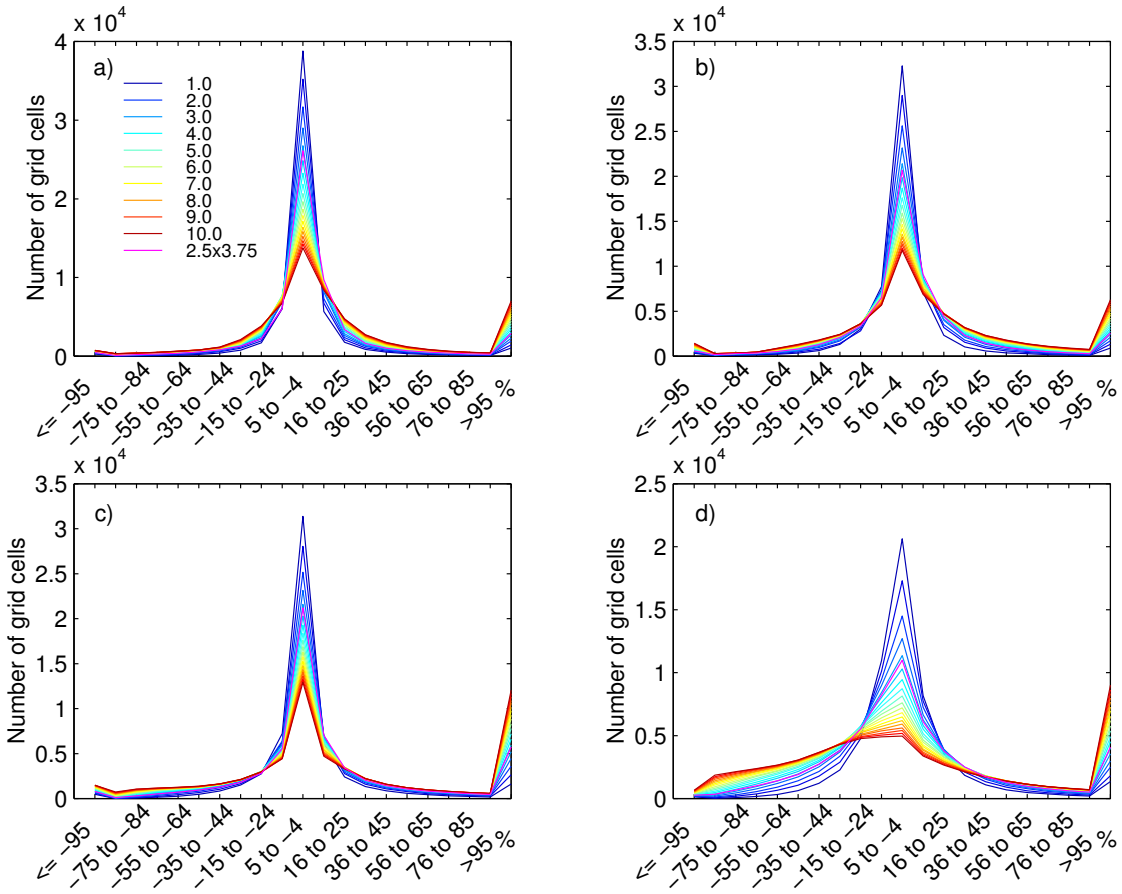

Supplementary figure S5. Histograms of difference between each 0.5° grid cell and their corresponding coarser grid cell in percent for water flows:
a) annual transpiration, b) annual evaporation, c) annual interception, and d) annual runoff.

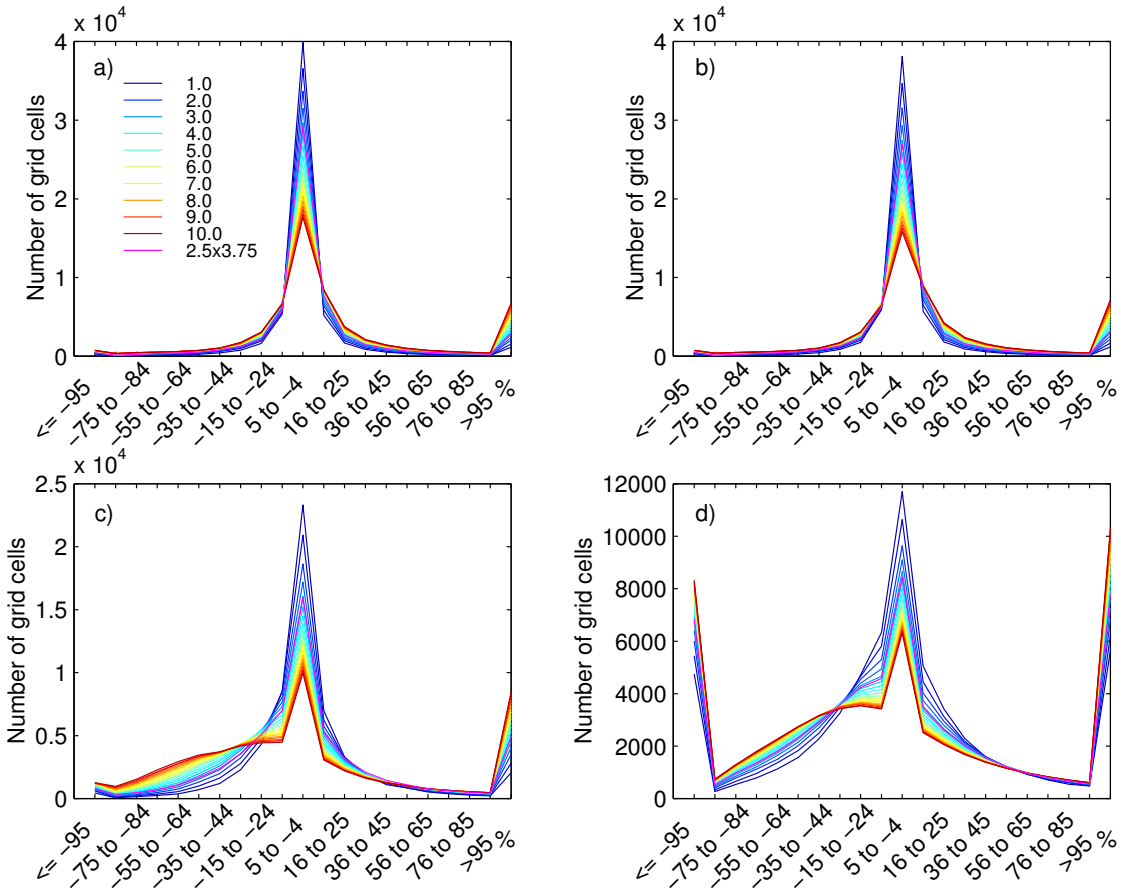

Supplementary figure S6. Histograms of difference between each 0.5° grid cell and their corresponding coarser grid cell in percent for carbon fluxes:
a) NPP, b) soil respiration (Rh), c) fire emissions, and d) NEE.

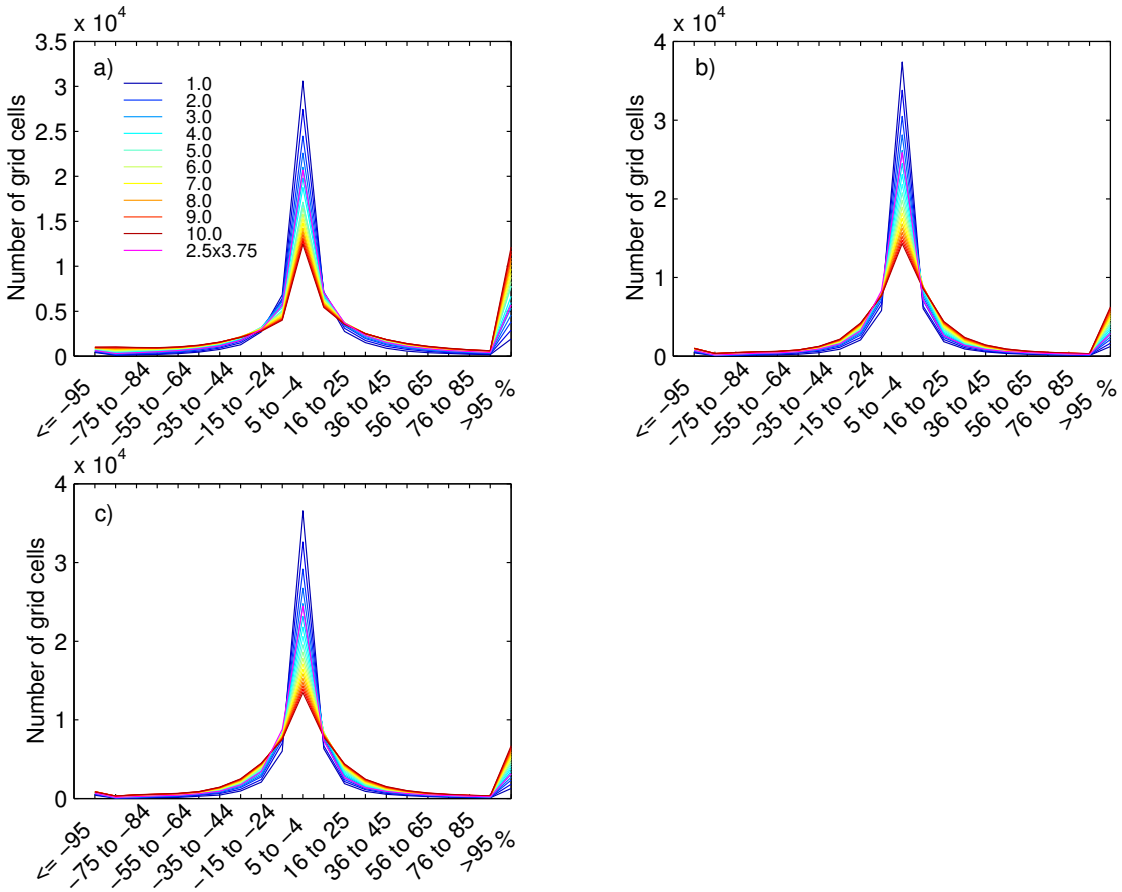

Supplementary figure S7. Histograms of difference between each 0.5° grid cell and their corresponding coarser grid cell in percent for carbon pools:
a) vegetation carbon, b) litter carbon, and c) soil carbon.

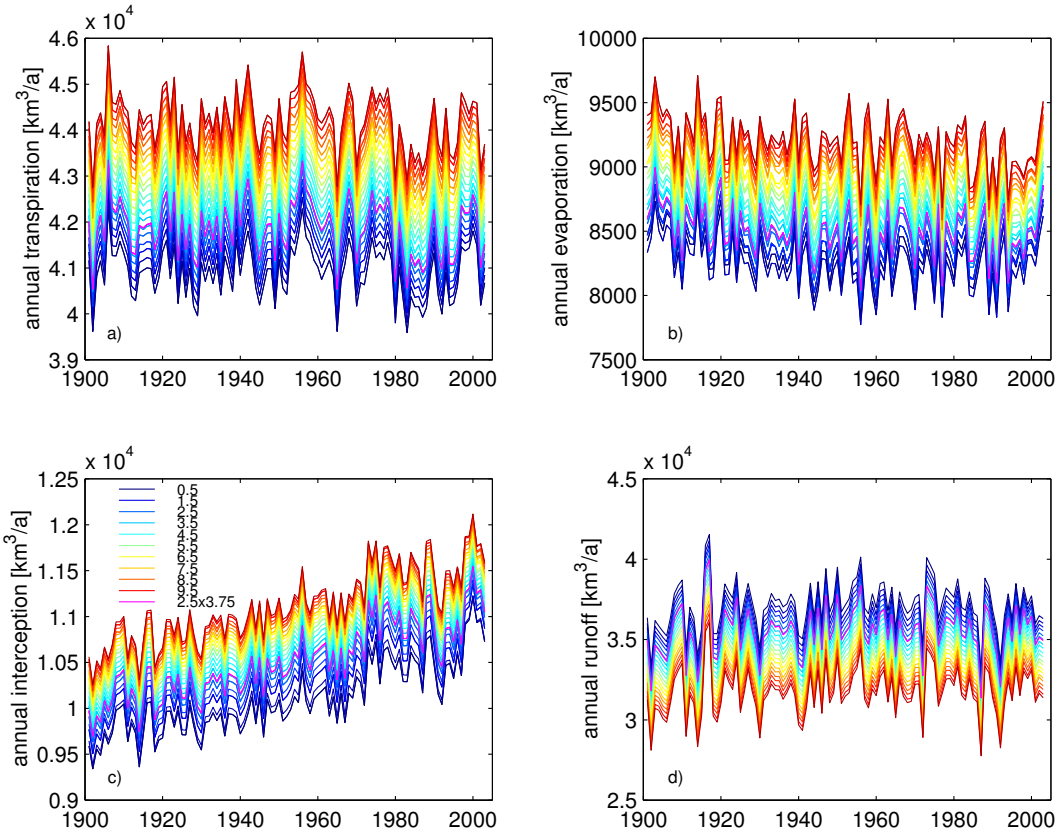

Supplementary figure S8. Time series of water flows at different resolutions:
a) annual transpiration, b) annual evaporation, c) annual interception, and d) annual runoff; all in km³/a.

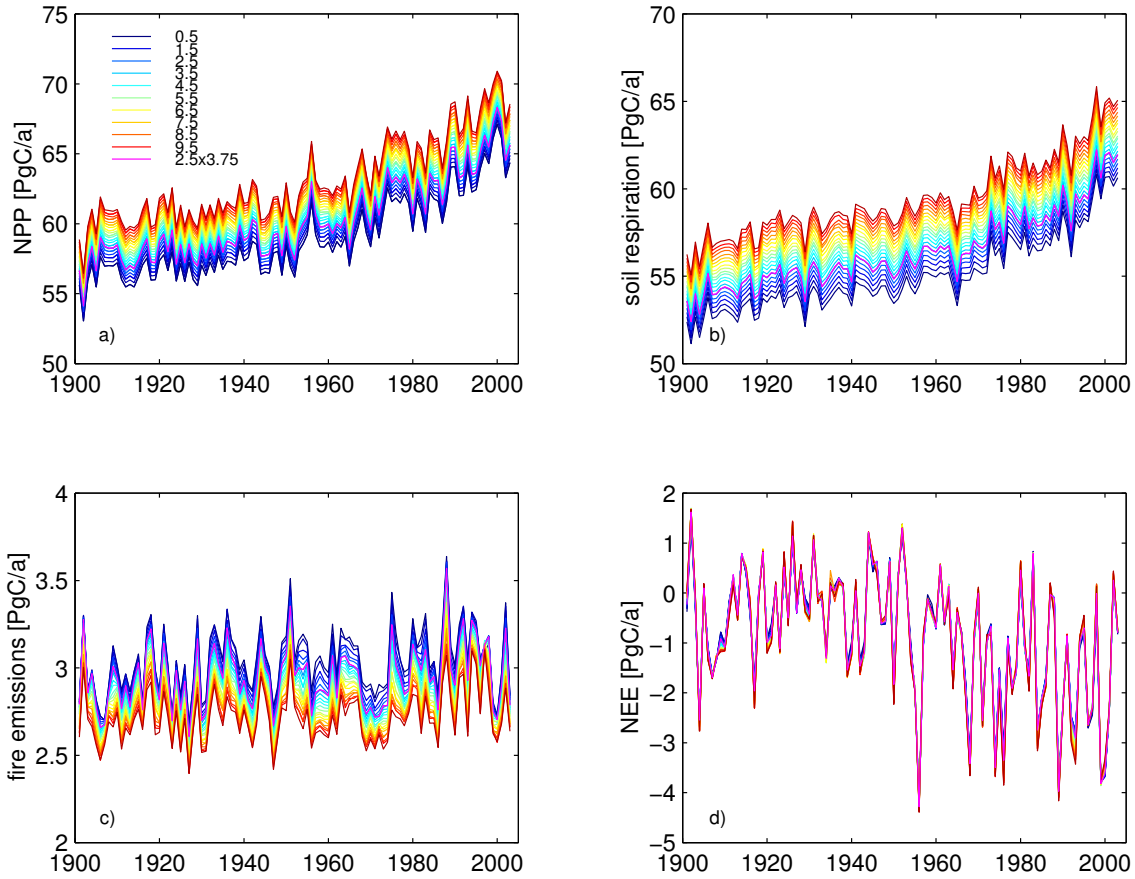

Supplementary figure S9. Time series of carbon fluxes at different resolutions:
a) NPP, b) soil respiration (R_h), c) fire emissions, and d) NEE; all in PgC/a.

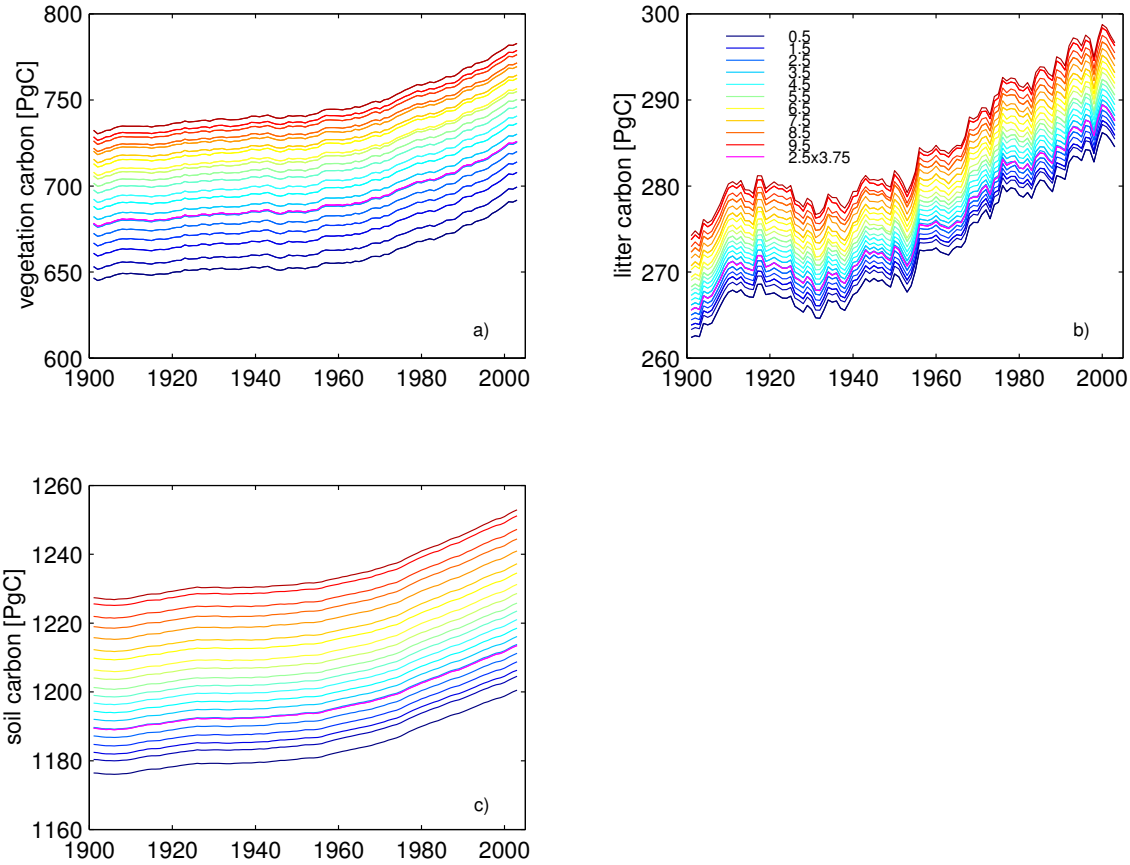

Supplementary figure S10. Time series of carbon pools at different resolutions: a) vegetation carbon, b) litter carbon, and c) soil carbon; all in PgC.

Table 1: Grid cells in regular grids

Resolution	Average number of cells (Range of alternative aggregations)	Computation time [% of benchmark]	Max. number of 0.5°x0.5° cells included
0.5 (benchmark)	59199	100.0	1
1.0	16039 (15965-16097)	27.0	4
1.5	7612 (7608-7620)	12.9	9
2.0	4506 (4498-4517)	7.6	16
2.5	3022 (3009-3035)	5.1	25
3.0	2192 (2186-2203)	3.7	36
3.5	1667 (1659-1675)	2.8	49
4.0	1319 (1308-1330)	2.2	64
4.5	1079 (1072-1084)	1.8	81
5.0	898 (894-901)	1.5	100
5.5	759 (756-762)	1.3	121
6.0	660 (655-665)	1.1	144
6.5	574 (569-580)	1.0	169
7.0	510 (506-515)	0.9	196
7.5	454 (446-457)	0.8	225
8.0	408 (405-412)	0.7	256
8.5	371 (369-374)	0.6	289
9.0	338 (334-342)	0.6	324
9.5	310 (306-313)	0.5	361
10.0	285 (278-289)	0.5	400
2.5x3.75	2112 (2093-2131)	3.6	40

Tab 2: Slope (deviation from benchmark value in percent per degree resolution) and coefficient of determination (R^2) for the regular grids of 0.5° to 10.0°. R^2 is computed with the intercept set to zero.

Model output [unit]	Slope	Coefficient of determination (R^2)
Soil carbon [PgC]	0.449	0.996
Litter carbon [PgC]	0.480	0.997
Vegetation carbon [PgC]	1.364	0.981
Annual transpiration [km³/a]	0.829	1.000
Annual evaporation [km³/a]	1.123	0.991
Annual interception [km³/a]	0.982	0.969
Annual runoff [km³/a]	-1.491	0.999
NPP [PgC/a]	0.707	0.998
NEE [PgC/a]	0.511	0.770[1]
Rh [PgC/a]	0.812	0.998
Fire emissions [PgC/a]	-1.133	0.999

[1] Here, the intercept had to be forced to zero, reducing the R^2.

Tab 3: Correlation coefficients (r) between the benchmark pattern and the spatial patterns at coarser resolutions.

Resolution [degrees]	Annual transpiration	Annual evaporation	Annual interception	Annual runoff	NPP	Soil respiration	Fire emissions	NEE	Litter carbon	Soil carbon	Vegetation carbon
0.5	1.000	1.000	1.000	1.000	1.000	1.000	1.000	1.000	1.000	1.000	1.000
1.0	0.996	0.962	0.991	0.982	0.990	0.989	0.943	0.762	0.981	0.982	0.982
1.5	0.992	0.937	0.986	0.972	0.983	0.983	0.915	0.739	0.968	0.968	0.971
2.0	0.988	0.920	0.981	0.962	0.977	0.977	0.895	0.681	0.959	0.959	0.962
2.5	0.985	0.901	0.975	0.951	0.972	0.972	0.877	0.657	0.951	0.950	0.952
3.0	0.981	0.889	0.971	0.942	0.966	0.966	0.855	0.631	0.939	0.939	0.946
3.5	0.978	0.872	0.966	0.933	0.961	0.961	0.840	0.610	0.936	0.936	0.938
4.0	0.974	0.858	0.961	0.926	0.954	0.954	0.821	0.598	0.929	0.928	0.929
4.5	0.968	0.843	0.957	0.919	0.949	0.949	0.799	0.567	0.920	0.922	0.921
5.0	0.965	0.824	0.952	0.907	0.943	0.943	0.789	0.548	0.912	0.913	0.911
5.5	0.960	0.818	0.949	0.904	0.939	0.939	0.781	0.525	0.912	0.912	0.911
6.0	0.955	0.801	0.943	0.889	0.931	0.930	0.762	0.518	0.897	0.899	0.900
6.5	0.955	0.788	0.940	0.887	0.930	0.930	0.753	0.457	0.892	0.896	0.900
7.0	0.945	0.763	0.930	0.873	0.917	0.917	0.747	0.481	0.879	0.883	0.884
7.5	0.942	0.740	0.926	0.870	0.912	0.912	0.720	0.426	0.883	0.883	0.879
8.0	0.940	0.754	0.924	0.862	0.906	0.906	0.715	0.451	0.882	0.885	0.877
8.5	0.937	0.733	0.923	0.860	0.904	0.904	0.714	0.418	0.851	0.852	0.871
9.0	0.929	0.726	0.916	0.851	0.890	0.890	0.692	0.470	0.850	0.853	0.864
9.5	0.931	0.705	0.912	0.853	0.900	0.901	0.696	0.463	0.863	0.860	0.851
10.0	0.917	0.703	0.902	0.831	0.877	0.876	0.671	0.420	0.835	0.840	0.854